Estimating global ammonia (NH_3) emissions based on IASI observations from 2008 to 2018

Zhenqi Luo[1, 2], Yuzhong Zhang[1, 2, *], Wei Chen[1, 2], Martin van Damme[3, 4], Pierre-François Coheur[3], Lieven Clarisse[3]

[1]Key Laboratory of Coastal Environment and Resources of Zhejiang Province, School of Engineering, Westlake University, Hangzhou, Zhejiang Province, 310024, China
[2]Institute of Advanced Technology, Westlake Institute for Advanced Study, Hangzhou, Zhejiang Province, 310024, China
[3]Université libre de Bruxelles (ULB), Spectroscopy, Quantum Chemistry and Atmospheric Remote Sensing (SQUARES), Brussels, Belgium
[4]BIRA-IASB - Belgian Institute for Space Aeronomy, Brussels, Belgium

Correspondence to: Y. Zhang (zhangyuzhong@westlake.edu.cn), Z. Luo (zl725@cornell.edu)

Abstract. Emissions of ammonia (NH_3) to the atmosphere impact human health, climate, and ecosystems through their critical contributions to secondary aerosol formation. Estimation of NH_3 emissions is associated with large uncertainties because of inadequate knowledge about agricultural sources. Here, we use satellite observations from the Infrared Atmospheric Sounding Interferometer (IASI) and simulations from the GEOS-Chem model to constrain global NH_3 emissions over the period of 2008-2018. We update the prior NH_3 emission fluxes with the ratio between biases in simulated NH_3 concentrations and effective NH_3 lifetimes against the loss of the NH_x family. In contrast to about a factor of two discrepancies between top-down and bottom-up emissions found in previous studies, our method results in a global land NH_3 emission of 78 (70-92) Tg a^{-1}, ~30 % higher than the bottom-up estimates. Regionally, we find that the bottom-up inventory underestimates NH_3 emissions over South America and tropical Africa by 60-70 %, indicating under-representation of agricultural sources in these regions. We find a good agreement within 10 % between bottom-up and top-down estimates over the U.S., Europe, and eastern China. Our results also show significant increases in NH_3 emissions over India (13 % $decade^{-1}$), tropical Africa (33 % $decade^{-1}$), and South America (18 % $decade^{-1}$) during our study period, consistent with the intensifying agricultural activities in these regions in the past decade. We find that inclusion of sulfur dioxide (SO_2) column observed by satellite is crucial for more accurate inference of NH_3 emission trends over important source regions such as India and China where SO_2 emissions have changed rapidly in recent years.

1 Introduction

Emissions of ammonia (NH_3) to the atmosphere have critical implications for human health, climate, and ecosystems. As the main alkaline gas, NH_3 reacts with acidic products from precursors such as nitrogen oxides (NO_x) and sulfur dioxide (SO_2) to form fine particulate matter, which is a well-documented risk factor for human health, causing great welfare loss globally

Deleted: 79 (71-96
Formatted: Font color: Red
Deleted: the
Formatted: Font: 宋体
Formatted: Font color: Red
Deleted: has
Formatted: Font color: Red
Formatted: Font color: Red
Formatted: Font color: Red
Formatted: Font color: Red
Formatted: Font color: Red
Deleted: matters
Formatted: Font color: Red

(Erisman 2021; Gu et al., 2021). Particulate matter also affects the Earth's radiative balance by directly scattering incoming radiation (Ma et al., 2012) and indirectly as cloud condensation nuclei (Höpfner et al., 2019). Additionally, both gas-phase ammonia (NH_3) and aerosol-phase ammonium (NH_4^+) can deposit onto the surface of land and water through dry and wet processes, and are associated with soil acidification (Zhao et al., 2009), ecosystem eutrophication (Dirnböck et al., 2013), biodiversity loss (Stevens et al., 2010), and cropland nitrogen uptake (Liu et al., 2013).

NH_3 is emitted from a variety of anthropogenic and natural sources, including agriculture, industry, fossil fuel combustion, biomass burning, natural soils, ocean, and wild animals (Behera et al., 2013). Among these, agricultural activities, mainly livestock manure management and mineral fertilizer application, are the most important NH_3 sources, which account for ~70% of the total NH_3 emissions globally (Bouwman et al., 1997; Sutton et al., 2013). NH_3 emissions can be estimated with a bottom-up approach based on information of emission activities and emission factors (Hoesly et al., 2018; Crippa et al., 2021). However, bottom-up estimates of NH_3 emissions are generally thought to be uncertain, relative to other pollutants that are mainly from fossil fuel combustion sources (e.g., NO_x, CO). One of the challenges is that the intensity of agricultural NH_3 emissions, emission factors, either from livestock or fertilizer, depends strongly on management and farming practices, but this information is usually not widely available (Zhang et al., 2017). Furthermore, microbial activities that are responsible for agricultural NH_3 emissions are highly variable and has a complex dependence on environmental conditions, which is often inadequately captured by bottom-up approaches (Behera et al., 2013; Vira et al., 2021). In many cases, emission factors used in bottom-up modelling are based on local studies that are not representative for the diversity of conditions and are not dependent on meteorological parameters.

Top-down analyses of atmospheric observations (e.g., NH_3 concentrations or NH_4^+ depositional fluxes) provide an alternative constraint on NH_3 emissions. For example, observations of NH_3 concentrations and NH_4^+ deposition fluxes from surface networks can be used to infer regional NH_3 emission fluxes (e.g., Paulot et al., 2014). However, surface sites are often sparse, especially in developing continents such as Africa and South America, limiting our capability to constrain NH_3 emissions globally. The advent of satellite observations makes it possible to investigate long-term spatially resolved NH_3 emissions from national, continental, to global scales. Van Damme et al. (2018) reported large NH_3 point sources across the globe that are detected by the Infrared Atmospheric Sounding Interferometer (IASI) instrument but missing in the bottom-up inventories. Studies have also applied satellite data (e.g., IASI and Cross-track Infrared Sounder (CrIS)) to study NH_3 emissions from important source regions, including the U.S. (Cao et al., 2020; Chen et al., 2021b), China (Zhang et al., 2018), and Europe (Marais et al., 2021; van der Graaf et al., 2021). These regional studies show 20 % to 50 % differences between top-down and bottom-up estimates of NH_3 emissions.

Compared to regional analyses, long-term global analyses of NH_3 emissions based on satellite observations are relatively scarce (e.g., Evangeliou et al., 2021). This is partly because of the computational challenges arising from a full-fledged inversion for a long period of time and over large spatial extents. In a recent study, Evangeliou et al. (2021) proposed a fast top-down method, in which NH_3 emissions are computed as the ratio between NH_3 column observations and NH_3 lifetime. This method relies on NH_3 lifetime diagnosed from a chemical transport model (CTM) and assumes a local mass balance.

Deleted: These particulate matters
Deleted: affect
Formatted: Font color: Red
Deleted: therefore
Formatted: Font color: Red
Formatted: Font color: Red
Deleted: depend
Deleted: depending

Their analysis found a global NH_3 emission of around 180 Tg a^{-1}, which is roughly triple the widely used bottom-up estimates (e.g., 62 Tg a^{-1} by the Community Emission Data System, CEDS). This large upward adjustment, if true, would have huge implications for global reactive nitrogen cycles and indicate that our current understanding of global NH_3 emissions is seriously flawed.

In this paper, we examine if the large discrepancy between the bottom-up and top-down estimates is due to the methodology. We refine the fast top-down approach by improving NH_3 lifetime diagnosis and partially accounting for the transport contributions. We develop a series of data filtering procedures to exclude results that are not sufficiently constrained by observations or affected by large deviations from the assumption of the fast top-down method. We apply the updated method to IASI observations to derive the global distribution of NH_3 emissions fluxes from 2008 to 2018, and examine the impact of the improved method on global NH_3 emission inferences.

2 Methods

2.1 IASI observations

We use 2008-2018 reanalyzed daily NH_3 total column retrievals (ANNI-NH_3-v3R) from the IASI on board Metop-A. The IASI instrument measures the infrared radiation (645–2760 cm^{-1}) from Earth's surface and the atmosphere with a circular 12 km footprint at nadir (Clerbaux et al., 2009; Van Damme et al., 2017). The retrieval algorithm calculates the hyperspectral range index from IASI spectra measurements (Van Damme et al. 2014) and converts it to the NH_3 total column density via an artificial neural network (Whitburn et al., 2016; Franco et al., 2018). The retrieval uses consistent meteorological data from the ERA5 reanalysis, so it is suitable for the analyses of inter-annual variability and long-term trends (Hersbach et al., 2020). The ANNI-NH_3-v3R product, has been validated against in situ measurements and is shown to have a good regional correlation (Guo et al., 2021; Van Damme et al., 2021). The dataset has been used in previous studies to estimate NH_3 emissions globally (e.g., Evangeliou et al., 2021) and regionally (e.g., Chen et al., 2021b; Marais et al., 2021).

Here we only use morning NH_3 data (around 9:30 local solar time) though IASI provides global coverage twice daily, because of the better precision of morning observations resulting from favourable thermal contrast conditions (Clarisse et al. 2010). We filter out data with a cloud fraction greater than 10 % (Van Damme et al., 2018) and a skin temperature below 263 K (Van Damme et al., 2014). The skin temperature dataset is from ERA5 (Hersbach et al., 2020). To compare with simulated NH_3 columns (see **Sect. 2.2**), we regrid and average monthly IASI NH_3 observations over land on the GEOS-Chem 4° × 5° grid (**Fig. 1a**). To reduce uncertainty from sparse sampling, we further exclude grid cells with the number of successful retrievals less than 800 in a month. We also test the choices of the threshold for 400 and 1200 per month in the sensitivity calculations (**Table 1**, line 5-6). This criterion affects mainly high latitudes during wintertime, where snow surfaces make it unfavourable for infrared measurements (**Fig. S1**).

Deleted: Finally, we evaluate the consistency of varied top-down and bottom-up estimates against IASI observations with full-chemistry simulations.¶

Formatted: Font color: Red, English (United States)

Formatted: Tab stops: 15.75 cm, Left

Deleted: favorable

Formatted: Font: +Body (Times New Roman)

Formatted: Font color: Red

Deleted: S1

Formatted: Font color: Red

Formatted: Font: 宋体, Font color: Red

Formatted: Font color: Red

Formatted: Font: Bold, Font color: Red

Formatted: Font color: Red

Formatted: Font: Bold, Font color: Red

Formatted: Font color: Red

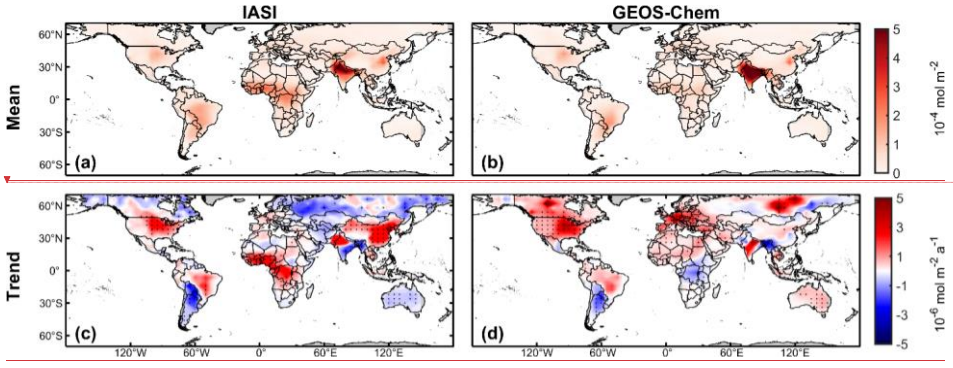

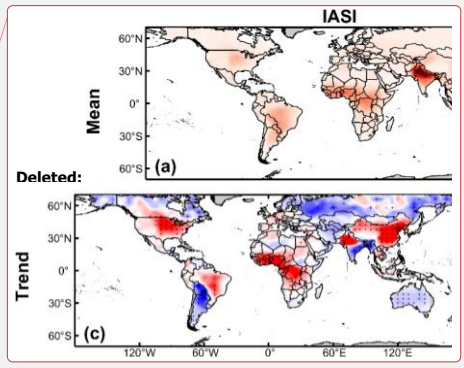

Deleted:

Figure 1. Spatial distribution of (a, c) IASI and (b, d) GEOS-Chem NH_3 column concentrations. (a, b) Mean and (c, d) linear trends within the **70**°N-**70**°S during 2008-2018. Dots in (c) and (d) indicate that linear trends are significant at the 95 % confidence levels. Linear trends are computed from the time series of annual averages.

2.2 GEOS-Chem simulations

We use the GEOS-Chem CTM v12.9.3 (10.5281/zenodo.3974569) to simulate global NH_3 concentrations. The GEOS-Chem model, driven by the MERRA-2 reanalyzed meteorology (Gelaro et al., 2017), simulates the tropospheric ozone–NOx–VOCs–aerosol chemistry at 4° × 5° resolution with 47 vertical layers (30 layers in the troposphere) (Bey et al., 2001; Park et al., 2004). The thermodynamic equilibrium between gas phase NH_3 and aerosol phase NH_4^+ is explicitly simulated by the ISORROPIA-II module in GEOS-Chem (Fountoukis & Nenes, 2007). The model also simulates the wet and dry deposition of NH_3 and NH_4^+, the terminal sinks of atmospheric NH_x (≡ NH_3 + NH_4^+). Dry deposition is represented with a resistances-in-series scheme (Wesely, 2007) and wet deposition includes scavenging in convective updrafts and in- and below-cloud scavenging from large-scale precipitation (Wang et al., 2011; Amos et al., 2012). Anthropogenic emissions of simulated chemicals including those of NH_3 are taken from a global emission inventory CEDS (Hoesly et al., 2018), overridden by regional inventories in Canada (Air Pollutant Emission Inventory, APEI), the United States (2011 National Emissions Inventory, NEI-2011), Asia (MIX-Asia v1.1) (Li et al., 2017), and Africa (DICE-Africa) (Eloise Marais and Christine Wiedinmyer, 2016). Such compiled anthropogenic emissions only include incomplete information on inter-annual trends because inventories are not all available throughout the whole period. Anthropogenic emissions are essentially invariant after 2013 in our setup (**Fig. S2**). The general lack of trends in SO_2 emissions in the simulation, if not accounted for, may cause biases in inferred trends over regions such as India and China where SO_2 emissions have changed rapidly (Sun et al., 2018; Qu et al., 2019; Chen et al., 2021a). Fire emissions are from Global Fire Emissions Database (GFED4) (van der Werf et al., 2017), and biogenic VOC emissions are from the Model of Emissions of Gases and Aerosols from Nature (MEGAN) (Guenther et al., 2012). Temporal (seasonal and inter-annual) variations in fire and biogenic emissions are resolved by the inventories. Hereafter, we refer to NH_3 prior bottom-up emissions from this set of inventories as BUE1. For comparison, we

Deleted: 错误!超链接引用无效。).

Deleted:).

Formatted: Font color: Red

Formatted: Font color: Red

also use another set of bottom-up inventories which consist of EDGARv5.0 for anthropogenic emissions (https://data.jrc.ec.europa.eu/collection/edgar, last access: 8 March 2022, Crippa et al., 2020), GFAS for fire emissions (CAMS, https://apps.ecmwf.int/datasets/data/cams-gfas/, last access: 8 March 2022) (minor natural emissions are the same as BUE1), which we denote as BUE2.

The GEOS-Chem simulation is conducted from 2008 to 2018 with an additional 1-month spin-up starting from December 2007. We sample the simulated NH_3 and NH_4^+ concentration fields between 9:00 to 10:00 local solar time, approximately the IASI morning overpass time. To compare with the IASI NH_3 columns, we integrate the vertical profiles of simulated NH_3 concentrations by layer thickness. We note that the ANNI-NH_3-v3R retrieval does not provide averaging kernels (Whitburn et al., 2016; Van Damme et al., 2021). However, Van Damme et al. (2018) reported the uncertainty in different vertical profiles of individual NH_3 measurements to be 2 % ± 24 % (global average). Besides, we also archive depositional and transport rates for NH_3 and NH_4^+, which are used in emission fluxes estimation. In addition, we perform GEOS-Chem simulations in selected years (2008, 2013, 2018) to examine the validation and consistency of our top-down NH_3 emission estimates with the ground-based measurements and IASI observations.

2.3 NH_3 emission fluxes estimation

We compute NH_3 fluxes ($\hat{E}_{NH_3}$, in molecules m^{-2} s^{-1}) in land grid cells for individual months from 2008 to 2018. We update the prior model emission fluxes ($E_{NH_3,mod}$, in molecules m^{-2} s^{-1}) with a correction term positively proportional to the difference of observed ($C_{NH_3,obs}$, in molecules m^{-2}) and simulated ($C_{NH_3,mod}$, in molecules m^{-2}) monthly averaged NH_3 total column densities and inversely proportional to the lifetime of NH_3 ($\tau_{NH_3,mod}$, in s):

$$\hat{E}_{NH_3} = E_{NH_3,mod} + \frac{C_{NH_3,obs} - C_{NH_3,mod}}{\tau_{NH_3,mod}}, \quad (1)$$

where $\tau_{NH_3,mod}$ is computed as the ratio of the simulated NH_3 column and the sum of simulated loss rate of the NH_x family ($NH_x \equiv NH_3 + NH_4^+$) through the dry and wet depositions of NH_3 ($D_{NH_3,mod}$, in molecules m^{-2} s^{-1}) and NH_4^+ ($D_{NH_4^+,mod}$, in molecules m^{-2} s^{-1}):

$$\tau_{NH_3,mod} = \frac{C_{NH_3,mod}}{D_{NH_3,mod} + D_{NH_4^+,mod}}. \quad (2)$$

Here we calculate the lifetime of NH_3 with the loss of the NH_x family rather than that of NH_3, because of the fast thermodynamic equilibrium between gas-phase NH_3 and aerosol/aqueous-phase NH_4^+, which implies that the conversion from NH_3 to NH_4^+ is not a terminal loss for NH_3 from the atmosphere. The NH_3 lifetime may be underestimated over source regions and overestimated over remote regions, if NH_3 to NH_4^+ conversions are treated as a terminal loss as in Evangeliou et al. (2021) rather than a partition within a chemical family (NH_x) as in **Eq. (2)**.

In addition, our method linearizes the column-emission relationship at prior emissions as opposed to zero emissions in the previous method (e.g., Evangeliou et al., 2021). Here, the baseline NH_3 column ($C_{NH_3,mod}$) simulated by the GEOS-Chem

Formatted ...
Formatted ...
Deleted: The
Deleted: algorithm
Deleted: information on the
Formatted ...
Formatted ...
Formatted ...
Deleted: sensitivity
Deleted: the IASI
Deleted: (i.e., averaging kernels) (错误!超链接引用无效。). In
Deleted:). In addition
Formatted ...
Formatted ...
Deleted: the top-down
Deleted: emission
Deleted: TDE) ($\hat{E}_{NH_3}$
Formatted ...
Formatted ...
Formatted ...
Formatted ...
Formatted ...
Deleted: consider
Formatted ...
Formatted ...
Formatted ...
Formatted ...
Formatted ...
Formatted ...
Formatted ...
Formatted ...
Formatted ...
Formatted ...
Formatted ...
Formatted ...
Formatted ...
Formatted ...
Formatted ...
Formatted ...
Formatted ...
Formatted ...
Formatted ...
Formatted ...
Formatted ...

model explicitly accounts for the non-local contribution of transport, while the correction to prior emissions is done only locally, that is, the difference between $C_{NH_3,obs}$ and $C_{NH_3,mod}$ is attributed only to errors in local emissions without accounting for the sensitivity to emissions from other grid cells. This hybrid approach can partially include the non-local contribution from transport but still keeps the computation tractable for a long-term study such as this study, striking a trade-off between the computational efficiency of a local mass balance method (e.g., Van Damme et al., 2018; Evangeliou et al., 2021) and the accuracy of a full-fledged inversion, such as the 4D-Var method (e.g., Cao et al., 2020; Chen et al., 2021b). The errors arising from local correction of NH_3 emissions are expected to be small in most cases, because the NH_3 lifetime is short relative to a typical transport time across a 4° × 5° grid cell on which emissions are estimated. To identify cases when this error is not negligible, we apply a monthly NH_x budget analysis based on the GEOS-Chem simulation and exclude grid cells from our analysis where transport dominates over local prior emissions or depositions in the monthly NH_x budget (Transport/Emission>1 or Transport/Deposition>1) (**Fig. S3**).

Because rapid changes in SO_2 emissions in eastern China and India, particularly after 2012, are not captured by our prior simulation (**Fig. S2**), the estimation of NH_3 emission trends using **Eq. (1)** may be biased over these regions. To address this issue, we further modify **Eq. (1)** to include observed trends in SO_2 column concentrations:

$$\hat{E}_{NH_3,SO_2-correct} = E_{NH_3,mod} + \frac{C_{NH_3,obs} - C_{NH_3,mod} + 2\omega C_{SO_4^{2-},mod}}{\tau_{NH_3,mod}}, \quad (3)$$

where ω (%) is the fractional changes of average SO_2 columns relative to the baseline year (i.e., 2012) over China or India and $C_{SO_4^{2-},mod}$ (molecules m^{-2} s^{-1}) is the simulated column densities of aerosol sulfate. Here, we specify a linear trend of -5 % a^{-1} for eastern China and 5 % a^{-1} for India between 2012 and 2018, based on values derived from the ozone monitoring instrument (OMI) and Ozone Mapping and Profiler Suite (OMPS) observations (Wang and Wang, 2020; Liu et al., 2018). We also test the impact of the uncertainty in ω on trend inferences over China and India. The factor 2 accounts for the fact that two molecules of NH_3 are required to neutralize one molecule of H_2SO_4. **Eq. (3)** only applies when NH_3 is in excess, a condition usually met in eastern China and India but not necessarily elsewhere (Lachatre et al., 2019; Acharja et al., 2022). Therefore, we only apply **Eq. (3)** to eastern China and India to understand the impact of changing SO_2 emissions on the inference of NH_3 emission trends. To use SO_2 observations systematically in NH_3 emission estimations requires further investigations.

2.4 Uncertainty and sensitivity analysis

We perform a series of perturbation and sensitivity experiments to assess the uncertainty of our estimates (**Table 1**. We perturb $C_{NH_3,mod}$ and $\tau_{NH_3,mod}$ in **Eq. (1)**. The perturbations to $\tau_{NH_3,mod}$ are set to be 50 % and 200 % (**Table 1**, Line 1-2). The perturbation to $C_{NH_3,mod}$ is set to be the standard deviation of monthly mean column concentrations ($\sigma_{C,obs}$) (**Table 1**, Line 3-4), which is given by:

Formatted: Font color: Red
Formatted: Font color: Red
Formatted: Font color: Red
Formatted: Font color: Red
Formatted: Font color: Red
Formatted: Font color: Red
Formatted: Font color: Red
Formatted: Font color: Red
Formatted: Font color: Red
Formatted: Font color: Red
Formatted: Font color: Red
Formatted: Font color: Red
Formatted: Font color: Red
Deleted: NH_3
Deleted:). We also test the impact of alternative thresholds (0.2 and 5) on NH_3 emission estimations (**Table S1**, Line 7-8). This procedure mostly affects remote regions where emissions are small, notably northern high latitudes)
Formatted: Font color: Red
Formatted: Font color: Red
Deleted: yr
Deleted: yr
Deleted: S1).
Formatted: Font color: Red
Deleted: S1
Formatted: Font color: Red
Deleted: S1
Formatted: Font color: Red
Deleted: related to the number of IASI measurements (n) and their measurement errorsgiven by
Formatted: Font color: Red

$$\sigma_{\mathrm{C,obs}} = \sqrt{\frac{\sum_{i=1}^{i=n}(\sigma_i \times \Omega_i)^2}{n-1}}, \quad (4)$$

where Ω_i (in mol m^{-2}) is the i^{th} NH_3 column measurement out of a total number of n observations in a grid cell during a month and σ_i is the relative error. We then use $\Omega \pm \sigma_{C,obs}$ to evaluate the effect of measurement errors in emission estimates (**Table 1**, Line 3-4). We compute results with alternative data filtering parameters (**Table 1**, Line 5-8), including the thresholds to exclude grid cells when the number of observations is too small (**Table 1**, line 5-6) and the local mass balance assumption is potentially invalid (**Table 1**, Line 7-8). We also test if our trend inferences over China and India using Eq. (3) is sensitive to uncertainty in observed trends in SO_2 concentrations (ω_i).

Table 1. Uncertainty and sensitivity analyses of top-down NH_3 emissions. Annual averaged NH_3 emissions are summed over global land areas for 2008–2018.

	Parameter perturbed	Average emission (Tg a^{-1})
0	None [a] (TDE)	78
1	Halved NH_3 lifetime[b]	92
2	Doubled NH_3 lifetime[c]	70
3	Upper IASI column error	83
4	Lower IASI column error	72
5	Number of retrievals > 400[d]	81
6	Number of retrievals > 1200[e]	74
7	Transport/Emission < 0.2[f]	72
8	Transport/Emission < 5[g]	84

[a]Excluding a grid cell if retrieval number is less than 800 during a month, or transport dominates over emissions or depositions in the simulated monthly NH_3 budget.

[b-c]The lifetime is 50 % and 200 % of values from Eq. (1), respectively.

[d-e]Monthly retrieval number threshold for including a grid cell is set to be 400 and 1200, respectively.

[f-g]Local budget ratio the threshold for including a grid cell is set to be 0.2 and 5, respectively.

3 Results and discussion

3.1 Observed and simulated NH_3 concentrations

Fig. 1a and 1b plot observed and simulated NH_3 total column concentrations averaged over 2008-2018. The GEOS-Chem simulation generally reproduces the global distribution of NH_3 concentrations observed by the IASI instrument. Good agreements (i.e., difference < 10 %) are found in the U.S., Europe, and southern South America. Meanwhile, the GEOS-

Deleted: reported in the IASI product.

Formatted: Font color: Red

Formatted: Font color: Red

Formatted: Font color: Red

Deleted: **S1**, Line 3-4). We also conduct sensitivity tests by using alternative parameters in data filtering (**Table S1**, Line 5-8…

Formatted: Font color: Red

Formatted: Font color: Red

Formatted: English (United States)

Deleted: In addition, we perform GEOS-Chem full chemistry simulations in selected years (2008, 2013, 2018) to examine the consistency of NH_3 emission estimates with the IASI observations. We use our top-down estimate (TDE) and prior emissions (BUE1) to drive the full chemistry simulation. We compute the fractional biases (FBs) of these simulations against the IASI observations to evaluate the systematic biases in the resulting NH_3 column density fields:¶

$FB =$

Chem model underestimates NH_3 concentrations in eastern China, northern South America, and tropical Africa by 20-120 %, and overestimates in southern India by around 50 %, indicating biases in NH_3 emissions over these regions.

Fig. 1c and 1d show 2008-2018 linear trends in NH_3 column concentrations derived from the IASI observations and the GEOS-Chem simulations. The linear trends are computed based on the time series of annual averages. The IASI trends shown in Fig. 1c are in general consistent with a recent analysis by Van Damme et al. (2021). IASI observes a positive NH_3 concentration trend of 2.9 % a^{-1} over the U.S., and this trend is well captured by GEOS-Chem. Similarly, the observation and the simulation agree on a dipole pattern in South America (i.e., positive trend in Brazil and negative trend in Argentina). Because anthropogenic emissions over this region are set to be invariant in our simulation (**Fig. S2**), this agreement suggests that these trends are due to meteorological conditions and/or fire emissions, rather than changes in anthropogenic emissions. The satellite also observes significant positive trends in NH_3 concentrations over China (5.2 % a^{-1}) and tropical Africa (2.0 % a^{-1}), but these trends are not reproduced in the simulation (0.3 % a^{-1} for China and 0.2 % a^{-1} for tropical Africa). These simulation-observation differences can not only reflect discrepancies in the trends of anthropogenic NH_3 emissions, but also be attributed to uncaptured changes in SO_2 and/or NO_x emissions in these regions. We also find that a positive NH_3 concentration trend over Europe appears in the simulation (3.0 % a^{-1}) but is much weaker (1.0 % a^{-1}) in the observation, suggesting decreasing emissions after 2013. Satellite data shows positive NH_3 concentration trends in north-western India but negative trends in in south-eastern India which are not reproduced by the simulation, though these trends over India are mostly insignificant (at the 95 % confidence level) except for a few grid cells in the Southeast. Strong GEOS-Chem trends in eastern Canada and Siberia result from large wildfires that occurred in the latter part of the study period. IASI trends in northern boreal regions are less robust because of noisy and sparse measurements over high latitudes (**Fig. S1** and **Fig. S3**).

3.2 NH_3 emissions inferred from IASI observations

Fig. 2 shows the spatial distributions of NH_3 emission fluxes and their 2008–2018 linear trends inferred from IASI observations using the method described in **Sect. 2.3**. **Fig. 3** plots annual time series aggregated for seven selected regions. The top-down emission (TDE) estimates suggest upward adjustments in NH_3 emissions over South America (SA) by 62 %, tropical Africa (TA) by 69 %, and Central Asia (CA) by 327 %, relative to the prior inventory (BUE1), but downward adjustments in NH_3 emissions by 14 % in India Peninsula (IP) and by 33 % in Canada. After accounting for the contributions from natural emissions including fires, we find that most of these biases in NH_3 emissions can be attributed to anthropogenic sources, except for Canada where the underestimation appears to relate to fire emissions. This result reflects a general inadequate representation of agricultural and industrial emissions from developing continents in current global emission inventories. The TDE finds good agreements with the BUE1 (difference within 10 %) over the U.S., Europe (EU), eastern China (EC) and Australia.

Formatted: Font color: Red

Deleted: Both the satellite and model do not find significant trends in NH_3 concentrations over India (absolute value less than 1 % yr-

Deleted:).

Formatted: Font color: Red

Formatted: Font color: Red

Formatted: Font color: Red

Formatted: Font: 宋体, Font color: Red

Formatted: Font color: Red

Deleted: estimate

Deleted: suggests

Formatted: Font color: Red

Formatted: Font color: Red

Formatted: Font color: Red

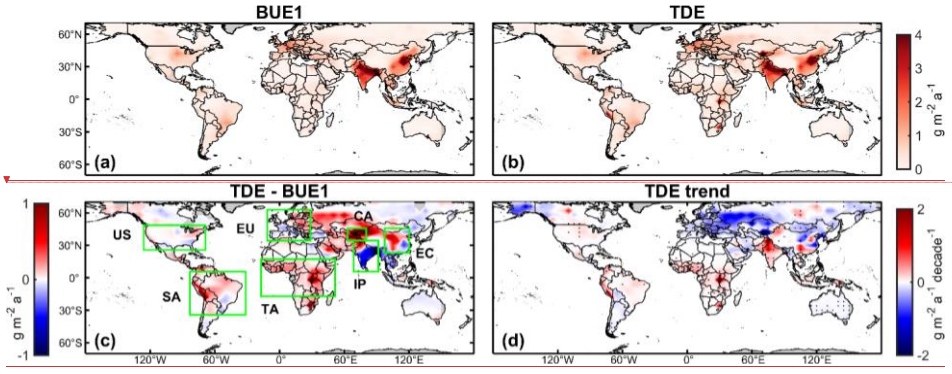

Figure 2. Spatial distribution of NH_3 emission fluxes during 2008-2018. (a) Bottom-up emissions (BUE1), (b) top-down emissions (TDE) inferred from IASI observations, (c) difference between TDE and BUE1 estimates and (d) emission trends derived from TDE estimates. Green boxes denote seven regions analyzed in Sect. 3.2. Top-down emission fluxes are computed with Eq. (1) except for IP and EC where Eq. (3) is applied. Linear trends are computed from the time series of annual averages. Dots in (d) represent significant linear trends at the 95 % confidence level.

In addition to the adjustments in average emissions, the TDE also detects changes in NH_3 emissions during the period of 2008-2018, as expressed in linear trends computed from annual time series. We find significant positive emission trends in SA (1.7 Tg a^{-1} $decade^{-1}$ or 18 % $decade^{-1}$) and TA (2.8 Tg a^{-1} $decade^{-1}$ or 33 % $decade^{-1}$) (**Fig. 3**). The large positive trends in TA are found around Lake Natron, consistent with Clarisse et al. (2019) (Fig. 2d). These increases in NH_3 emissions are concurrent with intensifying agricultural activities in these regions (Warner et al., 2017; E. Hickman et al., 2020), except for a 2010 peak over SA, which coincides with fires in savanna and evergreen forests there (Chen et al., 2013). Comparison with data from the Food and Agriculture Organization of the United Nations (FAO) (http://www.fao.org/faostat, last access: 7 May 2022) suggests that the increase in SA is driven primarily by growing application of synthetic fertilizer (55 % $decade^{-1}$), whereas the increase in TA is consistent with increasing manure amount (28 % $decade^{-1}$) from a growing livestock population (E. Hickman et al., 2021) (**Fig. 4**).

Our results infer large but variable trends over northern high latitudes (e.g., negative trends in Alaska, central Russia, and eastern Europe, but positive trends in Canada) (**Fig. 2d**). Because of large uncertainties associated with high-latitude observations and emission optimization, these trends are less robust but can be partly attributed to variations in fire activities. Decreases in Russia and eastern Europe are related to wildfire of boreal forests in early part of the study period (2008-2011) (Keywood et al., 2012; Warner et al., 2017), while emission increases in Canada is due to wildfire in the late part of the period (2013-2016 and 2017) (Pavlovic et al., 2016), as also shown in the prior fire inventory (GFED4) (**Fig. S4**). We also infer negative trends (-43 % $decade^{-1}$) in Australia, which are statistically significant, but the absolute magnitude of these trends is small (-0.03 g m^{-2} a^{-1} $decade^{-1}$ in **Fig. 2d**). The TDE estimation does not find significant trends in NH_3 total emissions over the US and Central Asia.

Deleted: analysed

Deleted: These increases

Formatted: Font color: Red

Formatted: Font color: Red

Deleted: July 2021

Formatted: Font color: Red

Formatted: Font color: Red

Moved (insertion) [1]

Moved (insertion) [2]

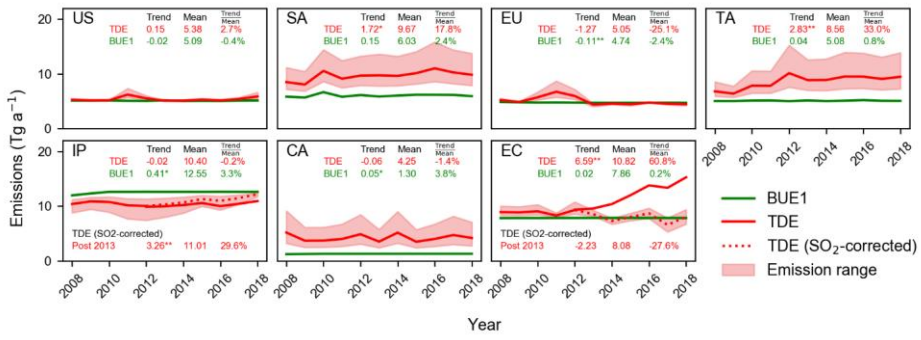

Figure 3. Annual NH_3 emissions for seven selected regions during 2008-2018. Shadings represent the upper and lower bounds derived from uncertainty analyses (see Sect. 2.4). Average annual emissions (Tg a^{-1}), absolute linear trends (Tg a^{-1} $decade^{-1}$) and relative trends (% $decade^{-1}$) for 2008-2018 are inset. The asterisk symbols '*' and '**' represent that linear trends are significant at the 95 % and 99 % confidence level, respectively. Red dashed lines represent top-down NH_3 emission estimates over IP and EC during 2013-2018, based on Eq. (3) that accounts for observed trends of SO_2 (denoted as "SO_2-corrected"). Statistics for this estimate are also inset. The prior inventory (BUE1) implemented in our simulation only partially account for inter-annual changes from bottom-up information (i.e., **Fig. 4**).

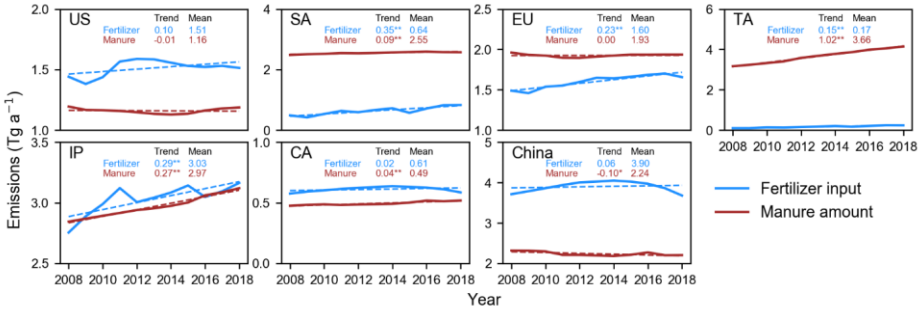

Figure 4. Synthetic fertilizer and livestock manure amount based on FAO reports (http://www.fao.org/faostat) during 2008-2018. To roughly compare the contribution from the two sectors, we convert FAO reported statistics to NH_3 emissions (Tg a^{-1}) by applying fixed emission factors of 13 % for manure N contents (Ma et al., 2020) and 17 % for synthetic fertilizer N contents (Riddick et al., 2016). Values of means (Tg a^{-1}) and linear trends (Tg a^{-1} $decade^{-1}$) are inset. Scales differ between panels.

3.3 Impact of changing SO_2 emissions on NH_3 emission trends over eastern China and India

Based on NH_3 column measurements (**Eq. (1)**), we also find a decadal increase of 61 % $decade^{-1}$ (6.6 Tg a^{-1} $decade^{-1}$) in NH_3 emissions over eastern China (**Fig. 3**). This increase is especially large after 2013 and is driven mainly by increases of IASI NH_3 column concentration in eastern China (**Fig. 1c**). This large post-2013 increase is inconsistent with flat or even

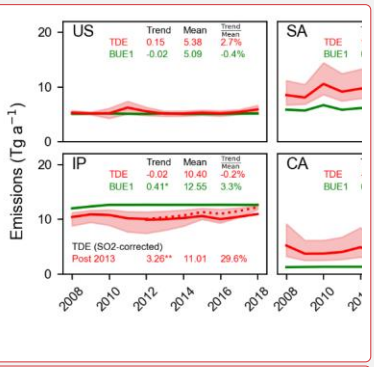

Deleted:

Deleted: range

Formatted: Font color: Red

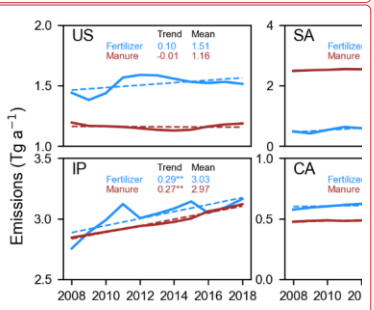

Deleted:

Deleted: management

Formatted: Font color: Red

Moved up [1]: Our results infer large but variable trends over northern high latitudes (e.g., negative trends in Alaska, central Russia, and eastern Europe, but positive trends in Canada) (**Fig. 2d**). Because of large uncertainties associated with high-latitude observations and emission optimization, these trends are less robust but can be partly attributed to variations in fire activities. Decreases

Moved up [2]: We also infer negative trends (-43 % $decade^{-1}$) in Australia, which are statistically significant, but the absolute magnitude of these trends is small (-0.03 g m^{-2} a^{-1} $decade^{-1}$ in **Fig.**

Deleted: 2015) (**错误!超链接引用无效。**).

Deleted:).

Deleted: only

Formatted: Font color: Red

Formatted: Font color: Red

declining fertilizer input and manure amount (**Fig. 4**). On the other hand, we find no appreciable emission trend in IP (**Fig. 3**), which appears to agree with relatively stable IASI NH_3 concentrations over the period (**Fig. 1c**) but is not supported by increases in fertilizer applications and manure amount shown in the FAO report (**Fig. 4**).

An assumption underlying **Eq. (1)** is that the model simulation captures the partition between gas-phase NH_3 and aerosol-phase NH_4^+. In addition to alkaline NH_3, the partition is also determined by the abundance of acids (e.g., H_2SO_4 and HNO_3). Inaccurate emissions of their precursors (e.g., SO_2 and NO_2) in the model simulation, in particular over regions with excessive NH_3, can lead to biases in simulating the NH_3-NH_4^+ partition. It is well known that SO_2 emissions in China have decreased rapidly after 2013 because of stringent air pollution control measures (Sun et al., 2018; Zhai et al., 2021), while SO_2 emissions from India have been increasing (Qu et al., 2019). But these regional trends are not captured in our prior simulation because our simulation does not have annual-varying emission inventories for these regions (**Fig. S2**).

We find that the discrepancies between top-down (**Eq. 1**) and bottom-up estimates of emission trends over EC and IP can be largely reconciled by including observed SO_2 column concentrations in the top-down calculation (**Eq. (3)**). By accounting for OMI and OMPS observed SO_2 trends (Wang and Wang, 2020), we derive an overall decreasing trend in NH_3 emissions in EC between 2013 and 2018 (-2.2 Tg a^{-1} $decade^{-1}$, -28 % $decade^{-1}$). This result suggests that observed increases in NH_3 columns over China are largely explained by decreases in SO_2 emissions (**Fig. 1** and **Fig. 3**), consistent with previous studies (Fu et al., 2017; Liu et al., 2018; Lachatre et al., 2019; Chen et al., 2021a). Bottom-up inventories (e.g., MEIC v1.3, EDGAR v5.0) also report stable or declining NH_3 emissions from China during the period (Li et al., 2017; Crippa et al., 2020). Meanwhile, the revised method (**Eq. (3)**) finds a positive post-2013 trend (3.3 Tg a^{-1} $decade^{-1}$, 30 % yr^{-1}) in NH_3 emissions over India. Compared with our original estimate using **Eq. (1)**, NH_3 emission trends derived with **Eq. (3)** (i.e., decrease in China and increase in India after 2013) is more consistent with the bottom-up information of fertilizer input and manure management (**Fig. 4**). This result demonstrates the potential of assimilating both NH_3 and SO_2 satellite observations in constraining NH_3 emissions, which should be further explored in the future.

3.4 Global total NH_3 emissions

Integrating over land areas globally, our IASI-based TDE estimates of NH_3 is 78 (70-92) Tg a^{-1} (range of estimates from uncertainty analysis, see **Table 1**) (**Fig. 5**). This result is about 20-40 % higher than bottom-up inventories (BUE1, 62 Tg a^{-1} and BUE2, 56 Tg a^{-1}). In contrast, a previous study by Evangeliou et al. (2021) also based on the IASI data estimated a much higher global NH_3 emission of 180 Tg a^{-1} (**Fig. 5**). One cause of the difference between the two IASI-based estimates is in diagnosis of NH_3 lifetime from CTM. Evangeliou et al. (2021) treats conversion from NH_3 to NH_4^+ as a terminal loss and diagnoses NH_3 lifetime averaged 11.6 ± 0.6 h globally from a CTM, which is close to a constant NH_3 lifetime (12 h) assumed in Van Damme et al. (2018). In this study, we account for the fact that fast thermodynamic equilibrium can establish between NH_3 and NH_4^+ so that NH_3 can only be terminally lost through the deposition of the NH_x family (**Eq. (2)**), which yields a global averaged NH_3 lifetime of 21.2 ± 3.8 h (**Fig. 6**). This longer NH_3 lifetime implies a higher sensitivity of NH_3 column density to NH_3 emissions, leading to a lower estimate for global NH_3 emissions. In addition, instead of locally

Deleted: due to a lack of
Deleted: data
Formatted: Font color: Red
Formatted: Font color: Red
Formatted: Font color: Red
Deleted: 3.4 Sensitivity of global emission inference to NH_3 lifetime diagnosis¶
Deleted: emissions
Deleted: 79 (71-96
Formatted: Font color: Red
Deleted: S1
Formatted: Font color: Red

scaling observed NH_3 column by lifetime (Van Damme et al., 2018; Evangeliou et al, 2021; Marais et al., 2021), our method (**Eq. (1)**) partially accounts for the non-local contribution from transport by including prior NH_3 columns from a full 3-D simulation and using their difference from observed NH_3 columns to correct prior emissions, which prevents derivation of large NH_3 emissions in remote regions where observed NH_3 concentrations are driven mainly by transport. Our data filtering strategy (**Sect 2.1 and 2.2**) is also crucial to avoid spurious top-down results when satellite coverage is poor and the local mass balance assumption does not hold.

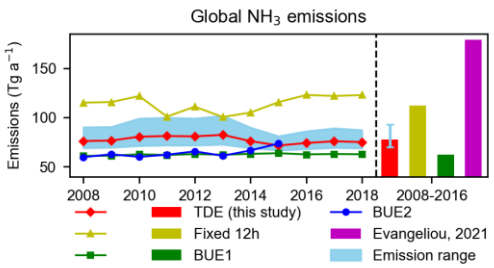

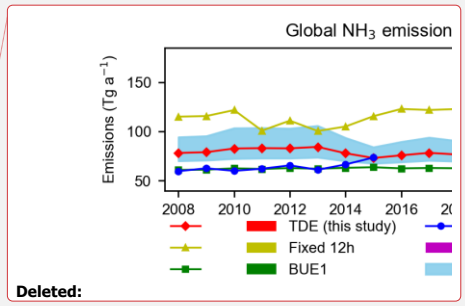

Deleted:

Figure 5. Comparison of our top-down NH_3 emission estimates (TDE) with other top-down (Fixed 12h and Evangeliou et al. (2021)) and bottom-up (BUE1 and BUE2) results during 2008-2018. The red line and red bar represent central estimates of the TDE, and the blue shaded area and the blue error bar indicate the uncertainty evaluated by our study (**Sect. 2.4**).

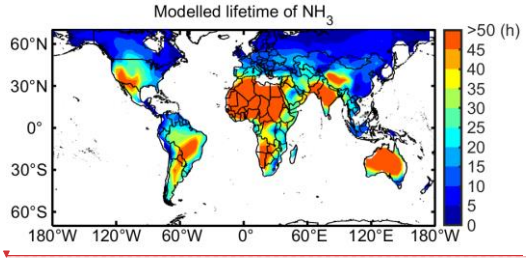

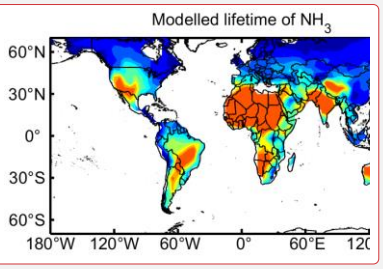

Deleted:

Figure 6. Spatial distribution of NH_3 lifetime (h) diagnosed from GEOS-Chem (Eq. (2)) within the $\mathbf{70^{\circ}}\boldsymbol{N}\text{-}\mathbf{70^{\circ}}\boldsymbol{S}$ during 2008-2018.

Fig. 6 shows the spatial variation in NH_3 lifetime diagnosed from the GEOS-Chem simulation. Short NH_3 lifetimes (< 10 h) are found mainly in northern high latitudes. Short lifetime in eastern China is due to high wet NH_4^+ deposition velocity, although some regional studies suggested an overestimation of deposition fluxes by the model especially in forest areas (e.g., Yangtze River basin) (Zhao et al., 2017; Xu et al., 2018). Very long NH_3 lifetime (> 100 h) occurs over Sahara and Australia, where dry conditions result in slow wet deposition.

3.5 Uncertainty evaluation

We derive the uncertainty of top-down estimates from the perturbation tests in **Table 1**. **Fig. 7** shows the global spatial distribution of annual average relative uncertainties of NH_3 emissions (ranges of perturbation tests divided by their averages). The relative uncertainties are large (up to >100%) over northern latitudes, Central Asia, northern Africa, and South America, where observations are often sparse. In comparison, the relative uncertainties are small (<40 %) in well-observed regions including eastern China, northern India, Europe, and the U.S.

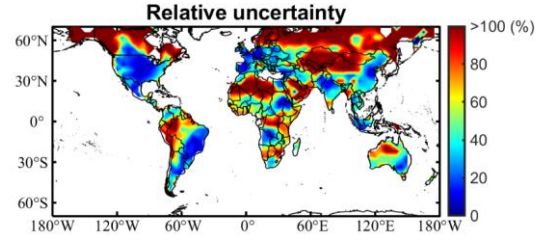

Figure 7. Spatial distribution of TDE relative uncertainty as the discrepancy of emission estimations in parameters perturbation **(Table 1)** divided by the TDE average during 2008-2018.

Our fast top-down method (Eq. (1) and Eq. (3)) relies on simplification of NH_3 chemical and physical processes. Therefore, it is not guaranteed that a simulation driven by TDE will generate results in improved agreement with IASI observations. We evaluate the consistency of our results using full GEOS-Chem simulations in the selected years of 2008, 2013, and 2018. Results are shown in **Fig. S5** (fractional bias, FB) and **Table S1** (number of valid grid cells, R^2, and root mean square error). The GEOS-Chem simulations driven by the prior emissions (BUE1) tends to underestimate NH_3 column density (mean FB ~-30%), while that driven by our TDE estimates achieves lower biases (mean FB ~10%), demonstrating the consistency of our TDE results with IASI observations.

We also compare simulated surface NH_3 concentrations with independent ground-based measurements from North America (AMoN, https://nadp.slh.wisc.edu/networks/ammonia-monitoring-network/, last access: 3 June 2022), Europe (EMEP, http://ebas-data.nilu.no/, last access: 3 June 2022), and South-eastern Asia (EANET, http://ebas-data.nilu.no/, last access: 3 June 2022). **Fig. 8** shows the comparison by season. Only small adjustments are inferred by our satellite-based estimations in these regions (i.e., North America, Europe, and South-eastern Asia). Thus, TDE and BUE1 show similar performance against these ground measurements. Although the simulation can capture the site-to-site variations reasonably well, simulated surface values are in general biased low compared to observations. This low bias is also reported in the evaluation of previous IASI-based estimates (e.g., Evangeliou et al, 2021; Chen et al., 2021b), which may be due to several reasons, for instance, systematic differences between satellite and surface measurements.

Deleted: We then evaluate the consistency of NH_3 emissions derived from varied methods with IASI observations3.

Formatted: Font color: Red

Deleted: 7

Deleted: S2

Formatted: Font color: Red

Formatted: Font color: Red

Deleted: full-chemistry

Formatted: Font color: Red

Formatted: Font color: Red

Deleted: emission

Deleted: with improved NH_3 lifetime calculation

Deleted: better consistency with observations

Deleted: %). The fact that

Formatted: Font color: Red

Formatted: Font color: Red

Formatted: Font color: Red

Formatted: Font color: Red

Deleted: is more consistent

Deleted: demonstrates the superiority of the improved top-down method.

Formatted: Font color: Red

Formatted: Font color: Red

Formatted: Font color: Red

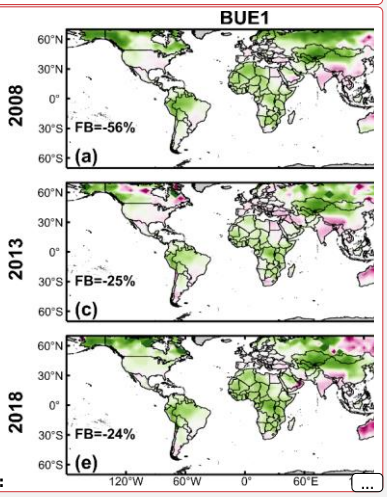

Deleted: ...

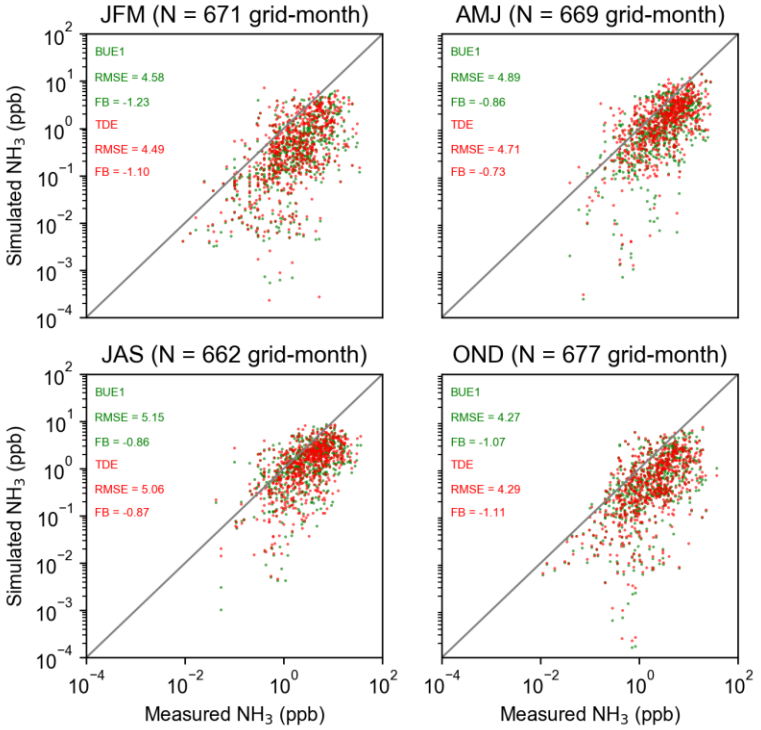

Figure 8. Validation of simulated NH_3 concentrations driven by BUE1 and TDE against ground-based measurements from AMoN, EMEP, EANET for selected years (2008, 2013 and 2018) in four seasons (January-March, JFM; April-June, AMJ; July-September, JAS; October-December, OND). Scatterplots are plotted in log scale and average RMSE (ppb) and FB (%) for each season are inset.

4 Conclusions

This study quantifies global ammonia (NH_3) fluxes monthly from 2008 to 2018 at 4° × 5° resolution, through a fast top-down method that incorporates IASI satellite observations and GEOS-Chem model simulations. The top-down method updates the prior NH_3 emissions with a correction term positively proportional to the difference of the observed and simulated NH_3 concentrations, and inversely proportional to the lifetime diagnosed from a CTM. This method revises previously proposed fast top-down methods in two aspects. First, we account for thermodynamic equilibrium within the NH_x family in diagnosing NH_3 lifetime, while previous studies either assume a globally constant lifetime or treat conversion from

NH_3 to NH_4^+ as a terminal sink. Second, our formulation linearizes the column-emission relationship at prior emissions as opposed to zero emissions in the previous method, which in general reduces errors from the local mass balance approximation. Another improvement is that we apply several data filtering procedures to exclude unreliable top-down results that are not sufficiently constrained by observations or affected by large deviations from the local mass balance assumption. The top-down method developed in this study is particularly useful for long-term global analysis of emission trends, because it largely accounts for the impact of meteorology through the CTM simulation and requires only small amount of computation relative to a full-fledged inversion.

We apply this improved fast top-down method to IASI NH_3 column observations from 2008 to 2018. We find that the BUE1 underestimates NH_3 emission over South America (62 %) and tropical Africa (69 %), but overestimates over India (14 %) and Canada (33 %). The bottom-up inventory agrees with the top-down estimate over the U.S., Europe, and eastern China (i.e., within 10 %). Our analysis also shows significant increases in India (13 % $decade^{-1}$), tropical Africa (33 % $decade^{-1}$), and South America (18 % $decade^{-1}$) during the study period, consistent with intensifying agricultural activities over these regions. An analysis of agricultural statistics suggests that the increase in tropical Africa is likely driven by growing livestock population and that in South America by increasing fertilizer usage.

We show that large increases in NH_3 concentrations in eastern China is mainly driven by rapid decreases in SO_2 emissions in recent years. By accounting for observed SO_2 columns, we find that NH_3 emissions from eastern China are significantly decreasing during 2008-2018 (-19 % $decade^{-1}$), with a larger negative trend after 2013 (-28 % $decade^{-1}$), as compared to a significant positive trend (61 % $decade^{-1}$) derived from assimilating only NH_3 data. Similarly, a lack of trend in observed NH_3 concentrations over India is due to concurrent increases in SO_2 and NH_3 emissions. After including observed SO_2 columns in the calculation, we estimate a 13 % increase in NH_3 emissions over India, with a significant post-2013 positive trend (30 % $decade^{-1}$). These results from assimilating both NH_3 and SO_2 data is more consistent with the agricultural statistics in China and India. The multi-satellite (SO_2 and NH_3) method is only applied in India and China in this study. To extend this idea globally requires development of formulations for varied sulfate-nitrate-ammonium aerosol regimes and needs to be addressed in a future study.

Our estimate for global total NH_3 emission is 78 (70-92) Tg a^{-1}, about 30 % higher than the BUE1 estimate. This contrasts with a much higher estimate (180 Tg a^{-1}) derived from Evangeliou et al. (2021) also using IASI data. The discrepancy can be primarily attributed to a longer NH_3 lifetime (i.e., global average 21 h) diagnosed in our method, which represents a greater sensitivity of NH_3 column to emissions, and a more conservative data filtering strategy, which removes potentially unreliable top-down results. Our diagnosis of NH_3 lifetime is an improvement over Evangeliou et al. (2021), by accounting for the thermodynamic equilibrium between gas phase NH_3 and aerosol phase NH_4^+ in our formula. We show with model simulations, our top-down estimate achieves better consistency with IASI observations, compared to the bottom-up emission inventory.

Formatted: Font color: Red

Deleted: bottom-up inventory (

Deleted:)

Deleted:

Deleted: is

Formatted: Font color: Red

Deleted: 79 (71-96

Formatted: Font color: Red

Deleted: full chemistry

Deleted: (BUE1).

Data availability.

The IASI L2 ammonia satellite observations are available at the AERIS data infrastructure (https://iasi.aeris-data.fr/). The ERA5 skin temperature and GFAS fire emission can be request through Copernicus Climate Data Store (https://cds.climate.copernicus.eu/cdsapp#!/home). Agricultural data are available through Food and Agriculture Organization of the United Nations (FAO) (http://www.fao.org/faostat). The GEOS-Chem model can be retrieved from 10.5281/zenodo.3974569. All the other data and scripts used for the present publication are available under MIT license on GitHub: https://github.com/bnulzq/NH3-emission.git and can be obtained from corresponding author upon request.

Author contributions.

ZL and YZ designed the study. ZL performed the simulations and analyses and wrote and coordinated the paper. WC contributed to the model simulations for consistency evaluation. LC, MVD, and PFC developed the IASI-NH3 satellite product. ZL and YZ wrote the paper with inputs from all authors.

Competing interests

The contact author has declared that neither they nor their co-authors have any competing interests.

Acknowledgements.

This study is supported by Westlake University. We thank the High-Performance Computing Center of Westlake University for the facility support and technical assistance. We acknowledge the AERIS data infrastructure https://www.aeris-data.fr for providing access to the IASI data. The IASI L1c data are received through the EUMETCast near real-time data distribution service. Research at ULB was supported by the Belgian State Federal Office for Scientific, Technical and Cultural Affairs (Prodex HIRS) and the Air Liquide Foundation (TAPIR project). LC is Research Associate supported by the Belgian F.R.S.-FNRS. Hersbach et al., (2020) was downloaded from the Copernicus Climate Change Service (C3S) Climate Data Store. The results contain modified Copernicus Climate Change Service information 2020. Neither the European Commission nor ECMWF is responsible for any use that may be made of the Copernicus information or data it contains. IASI is a join mission of Eumetsat and the "Centre National d'Études Spatiales" (CNES, France). We acknowledge the constructive comments and suggestions from Prof. Peter Hess from the Cornell University, Dr. Yi Wang from the University of Iowa, and Dr. Shixian Zhai from Harvard University. We also acknowledge Dr. Nikolaos Evangeliou from Norwegian Institute for Air Research for providing his NH_3 emission flux data and for discussions with ZL.

Deleted: the

Formatted: Font color: Red

Deleted: and

References

Acharja, P., Ali, K., Ghude, S. D., Sinha, V., Sinha, B., Kulkarni, R., Gultepe, I., and Rajeevan, M. N.: Enhanced secondary aerosol formation driven by excess ammonia during fog episodes in Delhi, India, Chemosphere, 289, 133155, 10.1016/j.chemosphere.2021.133155, 2022.

Amos, H. M., Jacob, D. J., Holmes, C. D., Fisher, J. A., Wang, Q., Yantosca, R. M., Corbitt, E. S., Galarneau, E., Rutter, A. P., Gustin, M. S., Steffen, A., Schauer, J. J., Graydon, J. A., Louis, V. L. S., Talbot, R. W., Edgerton, E. S., Zhang, Y., and Sunderland, E. M.: Gas-particle partitioning of atmospheric Hg(II) and its effect on global mercury deposition, Atmospheric Chemistry and Physics, 12, 591-603, 10.5194/acp-12-591-2012, 2012.

Behera, S. N., Sharma, M., Aneja, V. P., and Balasubramanian, R.: Ammonia in the atmosphere: a review on emission sources, atmospheric chemistry and deposition on terrestrial bodies, Environ Sci Pollut Res Int, 20, 8092-8131, 10.1007/s11356-013-2051-9, 2013.

Bey, I., Jacob, D. J., Yantosca, R. M., Logan, J. A., Field, B. D., Fiore, A. M., Li, Q., Liu, H. Y., Mickley, L. J., and Schultz, M. G.: Global modeling of tropospheric chemistry with assimilated meteorology: Model description and evaluation, Journal of Geophysical Research: Atmospheres, 106, 23073-23095, 10.1029/2001jd000807, 2001.

Bouwman, A. F., Lee, D. S., Asman, W. A. H., Dentener, F. J., Van Der Hoek, K. W., and Olivier, J. G. J.: A global high-resolution emission inventory for ammonia, Global Biogeochemical Cycles, 11, 561-587, 10.1029/97gb02266, 1997.

Cao, H., Henze, D. K., Shephard, M. W., Dammers, E., Cady-Pereira, K., Alvarado, M., Lonsdale, C., Luo, G., Yu, F., Zhu, L., Danielson, C. G., and Edgerton, E. S.: Inverse modeling of NH3 sources using CrIS remote sensing measurements, Environmental Research Letters, 15, 10.1088/1748-9326/abb5cc, 2020.

Chen, Y., Morton, D. C., Jin, Y., Collatz, G. J., Kasibhatla, P. S., van der Werf, G. R., DeFries, R. S., and Randerson, J. T.: Long-term trends and interannual variability of forest, savanna and agricultural fires in South America, Carbon Management, 4, 617-638, 10.4155/cmt.13.61, 2014.

Chen, Y., Zhang, L., Henze, D. K., Zhao, Y., Lu, X., Winiwarter, W., Guo, Y., Liu, X., Wen, Z., Pan, Y., and Song, Y.: Interannual variation of reactive nitrogen emissions and their impacts on PM2.5 air pollution in China during 2005–2015, Environmental Research Letters, 16, 10.1088/1748-9326/ac3695, 2021a.

Chen, Y., Shen, H., Kaiser, J., Hu, Y., Capps, S. L., Zhao, S., Hakami, A., Shih, J.-S., Pavur, G. K., Turner, M. D., Henze, D. K., Resler, J., Nenes, A., Napelenok, S. L., Bash, J. O., Fahey, K. M., Carmichael, G. R., Chai, T., Clarisse, L., Coheur, P.-F., Van Damme, M., and Russell, A. G.: High-resolution hybrid inversion of IASI ammonia columns to constrain US ammonia emissions using the CMAQ adjoint model, Atmospheric Chemistry and Physics, 21, 2067-2082, 10.5194/acp-21-2067-2021, 2021b.

Deleted: Acharja, P., Ali, K., Ghude, S. D., Sinha, V., Sinha, B., Kulkarni, R., Gultepe, I., and Rajeevan, M. N.: Enhanced secondary aerosol formation driven by excess ammonia during fog episodes in Delhi, India, Chemosphere, 289, 133155, 10.1016/j.chemosphere.2021.133155, 2022.¶
Amos, H. M., Jacob, D. J., Holmes, C. D., Fisher, J. A., Wang, Q., Yantosca, R. M., Corbitt, E. S., Galarneau, E., Rutter, A. P., Gustin, M. S., Steffen, A., Schauer, J. J., Graydon, J. A., Louis, V. L. S., Talbot, R. W., Edgerton, E. S., Zhang, Y., and Sunderland, E. M.: Gas-particle partitioning of atmospheric Hg(II) and its effect on global mercury deposition, Atmospheric Chemistry and Physics, 12, 591-603, 10.5194/acp-12-591-2012, 2012.¶
Behera, S. N., Sharma, M., Aneja, V. P., and Balasubramanian, R.: Ammonia in the atmosphere: a review on emission sources, atmospheric chemistry and deposition on terrestrial bodies, Environ Sci Pollut Res Int, 20, 8092-8131, 10.1007/s11356-013-2051-9, 2013.¶
Bey, I., Jacob, D. J., Yantosca, R. M., Logan, J. A., Field, B. D., Fiore, A. M., Li, Q., Liu, H. Y., Mickley, L. J., and Schultz, M. G.: Global modeling of tropospheric chemistry with assimilated meteorology: Model description and evaluation, Journal of Geophysical Research: Atmospheres, 106, 23073-23095, 10.1029/2001jd000807, 2001.¶
Bouwman, A. F., Lee, D. S., Asman, W. A. H., Dentener, F. J., Van Der Hoek, K. W., and Olivier, J. G. J.: A global high-resolution emission inventory for ammonia, Global Biogeochemical Cycles, 11, 561-587, 10.1029/97gb02266, 1997.¶
Cao, H., Henze, D. K., Shephard, M. W., Dammers, E., Cady-Pereira, K., Alvarado, M., Lonsdale, C., Luo, G., Yu, F., Zhu, L., Danielson, C. G., and Edgerton, E. S.: Inverse modeling of NH3 sources using CrIS remote sensing measurements, Environmental Research Letters, 15, 10.1088/1748-9326/abb5cc, 2020.¶
Chen, Y., Morton, D. C., Jin, Y., Collatz, G. J., Kasibhatla, P. S., van der Werf, G. R., DeFries, R. S., and Randerson, J. T.: Long-term trends and interannual variability of forest, savanna and agricultural fires in South America, Carbon Management, 4, 617-638, 10.4155/cmt.13.61, 2014.¶
Chen, Y., Zhang, L., Henze, D. K., Zhao, Y., Lu, X., Winiwarter, W., Guo, Y., Liu, X., Wen, Z., Pan, Y., and Song, Y.: Interannual variation of reactive nitrogen emissions and their impacts on PM2.5 air pollution in China during 2005–2015, Environmental Research Letters, 16, 10.1088/1748-9326/ac3695, 2021a.¶
Chen, Y., Shen, H., Kaiser, J., Hu, Y., Capps, S. L., Zhao, S., Hakami, A., Shih, J.-S., Pavur, G. K., Turner, M. D., Henze, D. K., Resler, J., Nenes, A., Napelenok, S. L., Bash, J. O., Fahey, K. M., Carmichael, G. R., Chai, T., Clarisse, L., Coheur, P.-F., Van Damme, M., and Russell, A. G.: High-resolution hybrid inversion of IASI ammonia columns to constrain US ammonia emissions using the CMAQ adjoint model, Atmospheric Chemistry and Physics, 21, 2067-2082, 10.5194/acp-21-2067-2021, 2021b.¶
Clerbaux, C., Boynard, A., Clarisse, L., George, M., Hadji-Lazaro, J., Herbin, H., Hurtmans, D., Pommier, M., Razavi, A., Turquety, S. J. A. C., and Physics: Monitoring of atmospheric composition using the thermal infrared IASI/MetOp sounder, Atmospheric Chemistry and Physics, 9, 6041-6054, 2009.¶
Crippa, M., Solazzo, E., Huang, G., Guizzardi, D., Koffi, E., Muntean, M., Schieberle, C., Friedrich, R., and Janssens-Maenhout, G.: High resolution temporal profiles in the Emissions Database for Global Atmospheric Research, Sci Data, 7, 121, 10.1038/s41597-020-0462-2, 2020.¶
Dirnbock, T., Grandin, U., Bernhardt-Romermann, M., Beudert, B., Canullo, R., Forsius, M., Grabner, M. T., Holmberg, M., Kleemola, S., Lundin, L., Mirtl, M., Neumann, M., Pompei, E., Salemaa, M., ...

Clarisse, L., Van Damme, M., Gardner, W., Coheur, P. F., Clerbaux, C., Whitburn, S., ... & Hurtmans, D. (2019). Atmospheric ammonia (NH_3) emanations from Lake Natron's saline mudflats. Scientific reports, 9(1), 1-12.

Clerbaux, C., Boynard, A., Clarisse, L., George, M., Hadji-Lazaro, J., Herbin, H., Hurtmans, D., Pommier, M., Razavi, A., Turquety, S. J. A. C., and Physics: Monitoring of atmospheric composition using the thermal infrared IASI/MetOp sounder, Atmospheric Chemistry and Physics, 9, 6041-6054, 2009.

Crippa, M., Solazzo, E., Huang, G., Guizzardi, D., Koffi, E., Muntean, M., Schieberle, C., Friedrich, R., and Janssens-Maenhout, G.: High resolution temporal profiles in the Emissions Database for Global Atmospheric Research, Sci Data, 7, 121, 10.1038/s41597-020-0462-2, 2020.

Dirnbock, T., Grandin, U., Bernhardt-Romermann, M., Beudert, B., Canullo, R., Forsius, M., Grabner, M. T., Holmberg, M., Kleemola, S., Lundin, L., Mirtl, M., Neumann, M., Pompei, E., Salemaa, M., Starlinger, F., Staszewski, T., and Uzieblo, A. K.: Forest floor vegetation response to nitrogen deposition in Europe, Glob Chang Biol, 20, 429-440, 10.1111/gcb.12440, 2014.

Erisman, J. W. J. S.: How ammonia feeds and pollutes the world, Science, 374, 685-686, 2021.

Evangeliou, N., Balkanski, Y., Eckhardt, S., Cozic, A., Van Damme, M., Coheur, P.-F., Clarisse, L., Shephard, M. W., Cady-Pereira, K. E., and Hauglustaine, D.: 10-year satellite-constrained fluxes of ammonia improve performance of chemistry transport models, Atmospheric Chemistry and Physics, 21, 4431-4451, 10.5194/acp-21-4431-2021, 2021.

Fountoukis, C., Nenes, A. J. A. C., and Physics: ISORROPIA II: a computationally efficient thermodynamic equilibrium model for K+–Ca 2+–Mg 2+–NH 4+–Na+–SO 4 2−–NO 3−–Cl−–H 2 O aerosols, Atmospheric Chemistry and Physics, 7, 4639-4659, 2007.

Franco, B., Clarisse, L., Stavrakou, T., Müller, J. F., Van Damme, M., Whitburn, S., Hadji‐Lazaro, J., Hurtmans, D., Taraborrelli, D., Clerbaux, C., and Coheur, P. F.: A General Framework for Global Retrievals of Trace Gases From IASI: Application to Methanol, Formic Acid, and PAN, Journal of Geophysical Research: Atmospheres, 123, 10.1029/2018jd029633, 2018.

Fu, X., Wang, S., Xing, J., Zhang, X., Wang, T., and Hao, J.: Increasing Ammonia Concentrations Reduce the Effectiveness of Particle Pollution Control Achieved via SO2 and NOX Emissions Reduction in East China, Environmental Science & Technology Letters, 4, 221-227, 10.1021/acs.estlett.7b00143, 2017.

Gelaro, R., McCarty, W., Suarez, M. J., Todling, R., Molod, A., Takacs, L., Randles, C., Darmenov, A., Bosilovich, M. G., Reichle, R., Wargan, K., Coy, L., Cullather, R., Draper, C., Akella, S., Buchard, V., Conaty, A., da Silva, A., Gu, W., Kim, G. K., Koster, R., Lucchesi, R., Merkova, D., Nielsen, J. E., Partyka, G., Pawson, S., Putman, W., Rienecker, M., Schubert, S. D., Sienkiewicz, M., and Zhao, B.: The Modern-Era Retrospective Analysis for Research and Applications, Version 2 (MERRA-2), J Clim, Volume 30, 5419-5454, 10.1175/JCLI-D-16-0758.1, 2017.

Gu, B., Zhang, L., Van Dingenen, R., Vieno, M., Van Grinsven, H. J., Zhang, X., Zhang, S., Chen, Y., Wang, S., and Ren, C. J. S.: Abating ammonia is more cost-effective than nitrogen oxides for mitigating PM2. 5 air pollution, Science, 374, 758-762, 2021.

Guenther, A. B., Jiang, X., Heald, C. L., Sakulyanontvittaya, T., Duhl, T., Emmons, L. K., and Wang, X.: The Model of Emissions of Gases and Aerosols from Nature version 2.1 (MEGAN2.1): an extended and updated framework for modeling biogenic emissions, Geoscientific Model Development, 5, 1471-1492, 10.5194/gmd-5-1471-2012, 2012.

Guo, X., Wang, R., Pan, D., Zondlo, M. A., Clarisse, L., Van Damme, M., Whitburn, S., Coheur, P. F., Clerbaux, C., Franco, B., Golston, L. M., Wendt, L., Sun, K., Tao, L., Miller, D., Mikoviny, T., Müller, M., Wisthaler, A., Tevlin, A. G., Murphy, J. G., Nowak, J. B., Roscioli, J. R., Volkamer, R., Kille, N., Neuman, J. A., Eilerman, S. J., Crawford, J. H., Yacovitch, T. I., Barrick, J. D., and Scarino, A. J.: Validation of IASI Satellite Ammonia Observations at the Pixel Scale Using In Situ Vertical Profiles, Journal of Geophysical Research: Atmospheres, 126, 10.1029/2020jd033475, 2021.

Hersbach, H., Bell, B., Berrisford, P., Hirahara, S., Horányi, A., Muñoz‐Sabater, J., Nicolas, J., Peubey, C., Radu, R., Schepers, D., Simmons, A., Soci, C., Abdalla, S., Abellan, X., Balsamo, G., Bechtold, P., Biavati, G., Bidlot, J., Bonavita, M., Chiara, G., Dahlgren, P., Dee, D., Diamantakis, M., Dragani, R., Flemming, J., Forbes, R., Fuentes, M., Geer, A., Haimberger, L., Healy, S., Hogan, R. J., Hólm, E., Janisková, M., Keeley, S., Laloyaux, P., Lopez, P., Lupu, C., Radnoti, G., Rosnay, P., Rozum, I., Vamborg, F., Villaume, S., and Thépaut, J. N.: The ERA5 global reanalysis, Quarterly Journal of the Royal Meteorological Society, 146, 1999-2049, 10.1002/qj.3803, 2020.

Hickman, J. E., Andela, N., Tsigaridis, K., Galy-Lacaux, C., Ossohou, M., and Bauer, S. E.: Reductions in NO2 burden over north equatorial Africa from decline in biomass burning in spite of growing fossil fuel use, 2005 to 2017, Proc Natl Acad Sci U S A, 118, 10.1073/pnas.2002579118, 2021a.

Hickman, J. E., Andela, N., Dammers, E., Clarisse, L., Coheur, P.-F., Van Damme, M., Di Vittorio, C. A., Ossohou, M., Galy-Lacaux, C., Tsigaridis, K., and Bauer, S. E.: Changes in biomass burning, wetland extent, or agriculture drive atmospheric NH_3; trends in select African regions, Atmospheric Chemistry and Physics, 21, 16277-16291, 10.5194/acp-21-16277-2021, 2021b.

Hoesly, R. M., Smith, S. J., Feng, L., Klimont, Z., Janssens-Maenhout, G., Pitkanen, T., Seibert, J. J., Vu, L., Andres, R. J., Bolt, R. M., Bond, T. C., Dawidowski, L., Kholod, N., Kurokawa, J.-i., Li, M., Liu, L., Lu, Z., Moura, M. C. P., O'Rourke, P. R., and Zhang, Q.: Historical (1750–2014) anthropogenic emissions of reactive gases and aerosols from the Community Emissions Data System (CEDS), Geoscientific Model Development, 11, 369-408, 10.5194/gmd-11-369-2018, 2018.

Höpfner, M., Ungermann, J., Borrmann, S., Wagner, R., Spang, R., Riese, M., Stiller, G., Appel, O., Batenburg, A. M., Bucci, S., Cairo, F., Dragoneas, A., Friedl-Vallon, F., Hünig, A., Johansson, S., Krasauskas, L., Legras, B., Leisner, T., Mahnke, C., Möhler, O., Molleker, S., Müller, R., Neubert, T., Orphal, J., Preusse, P., Rex, M., Saathoff, H., Stroh, F., Weigel, R., and Wohltmann, I.: Ammonium

nitrate particles formed in upper troposphere from ground ammonia sources during Asian monsoons, Nature Geoscience, 12, 608-612, 10.1038/s41561-019-0385-8, 2019.

Keywood, M., Kanakidou, M., Stohl, A., Dentener, F., Grassi, G., Meyer, C. P., Torseth, K., Edwards, D., Thompson, A. M., Lohmann, U., and Burrows, J.: Fire in the Air: Biomass Burning Impacts in a Changing Climate, Critical Reviews in Environmental Science and Technology, 43, 40-83, 10.1080/10643389.2011.604248, 2011.

Lachatre, M., Fortems-Cheiney, A., Foret, G., Siour, G., Dufour, G., Clarisse, L., Clerbaux, C., Coheur, P.-F., Van Damme, M., and Beekmann, M.: The unintended consequence of SO_2 and NO_2; regulations over China: increase of ammonia levels and impact on $PM_{2.5}$; concentrations, Atmospheric Chemistry and Physics, 19, 6701-6716, 10.5194/acp-19-6701-2019, 2019.

Li, M., Zhang, Q., Kurokawa, J.-i., Woo, J.-H., He, K., Lu, Z., Ohara, T., Song, Y., Streets, D. G., Carmichael, G. R., Cheng, Y., Hong, C., Huo, H., Jiang, X., Kang, S., Liu, F., Su, H., and Zheng, B.: MIX: a mosaic Asian anthropogenic emission inventory under the international collaboration framework of the MICS-Asia and HTAP, Atmospheric Chemistry and Physics, 17, 935-963, 10.5194/acp-17-935-2017, 2017.

Liu, M., Huang, X., Song, Y., Xu, T., Wang, S., Wu, Z., Hu, M., Zhang, L., Zhang, Q., Pan, Y., Liu, X., and Zhu, T.: Rapid SO_2; emission reductions significantly increase tropospheric ammonia concentrations over the North China Plain, Atmospheric Chemistry and Physics, 18, 17933-17943, 10.5194/acp-18-17933-2018, 2018.

Liu, X., Zhang, Y., Han, W., Tang, A., Shen, J., Cui, Z., Vitousek, P., Erisman, J. W., Goulding, K., Christie, P., Fangmeier, A., and Zhang, F.: Enhanced nitrogen deposition over China, Nature, 494, 459-462, 10.1038/nature11917, 2013.

Ma, R., Zou, J., Han, Z., Yu, K., Wu, S., Li, Z., Liu, S., Niu, S., Horwath, W. R., and Zhu-Barker, X.: Global soil-derived ammonia emissions from agricultural nitrogen fertilizer application: A refinement based on regional and crop-specific emission factors, Glob Chang Biol, 27, 855-867, 10.1111/gcb.15437, 2021.

Ma, X., Yu, F., and Luo, G.: Aerosol direct radiative forcing based on GEOS-Chem-APM and uncertainties, Atmospheric Chemistry and Physics, 12, 5563-5581, 10.5194/acp-12-5563-2012, 2012.

Marais, E. A. and Wiedinmyer, C.: Air Quality Impact of Diffuse and Inefficient Combustion Emissions in Africa (DICE-Africa), Environ Sci Technol, 50, 10739-10745, 10.1021/acs.est.6b02602, 2016.

Marais, E. A., Pandey, A. K., Van Damme, M., Clarisse, L., Coheur, P. F., Shephard, M. W., Cady‐Pereira, K. E., Misselbrook, T., Zhu, L., Luo, G., and Yu, F.: UK Ammonia Emissions Estimated With Satellite Observations and GEOS‐Chem, Journal of Geophysical Research: Atmospheres, 126, 10.1029/2021jd035237, 2021.

828 Park, R. J.: Natural and transboundary pollution influences on sulfate-nitrate-ammonium aerosols in the
829 United States: Implications for policy, Journal of Geophysical Research, 109, 10.1029/2003jd004473,
830 2004.

831 Paulot, F., Jacob, D. J., Pinder, R. W., Bash, J. O., Travis, K., and Henze, D. K.: Ammonia emissions in
832 the United States, European Union, and China derived by high-resolution inversion of ammonium wet
833 deposition data: Interpretation with a new agricultural emissions inventory (MASAGE_NH3), Journal
834 of Geophysical Research: Atmospheres, 119, 4343-4364, 10.1002/2013jd021130, 2014.

835 Pavlovic, R., Chen, J., Anderson, K., Moran, M. D., Beaulieu, P. A., Davignon, D., and Cousineau, S.:
836 The FireWork air quality forecast system with near-real-time biomass burning emissions: Recent
837 developments and evaluation of performance for the 2015 North American wildfire season, J Air Waste
838 Manag Assoc, 66, 819-841, 10.1080/10962247.2016.1158214, 2016.

839 Qu, Z., Henze, D. K., Li, C., Theys, N., Wang, Y., Wang, J., Wang, W., Han, J., Shim, C., Dickerson,
840 R. R., and Ren, X.: SO2 Emission Estimates Using OMI SO2 Retrievals for 2005-2017, J Geophys Res
841 Atmos, 124, 8336-8359, 10.1029/2019JD030243, 2019.

842 Riddick, S., Ward, D., Hess, P., Mahowald, N., Massad, R., and Holland, E.: Estimate of changes in
843 agricultural terrestrial nitrogen pathways and ammonia emissions from 1850 to present in the
844 Community Earth System Model, Biogeosciences, 13, 3397-3426, 10.5194/bg-13-3397-2016, 2016.

845 Schiferl, L. D., Heald, C. L., Van Damme, M., Clarisse, L., Clerbaux, C., Coheur, P.-F., Nowak, J. B.,
846 Neuman, J. A., Herndon, S. C., Roscioli, J. R., and Eilerman, S. J.: Interannual variability of ammonia
847 concentrations over the United States:

848 sources and implications, Atmospheric Chemistry and Physics, 16, 12305-12328, 10.5194/acp-16-
849 12305-2016, 2016.

850 Stevens, C. J., Dupre, C., Dorland, E., Gaudnik, C., Gowing, D. J., Bleeker, A., Diekmann, M., Alard,
851 D., Bobbink, R., Fowler, D., Corcket, E., Mountford, J. O., Vandvik, V., Aarrestad, P. A., Muller, S.,
852 and Dise, N. B.: Nitrogen deposition threatens species richness of grasslands across Europe, Environ
853 Pollut, 158, 2940-2945, 10.1016/j.envpol.2010.06.006, 2010.

854 Sun, W., Shao, M., Granier, C., Liu, Y., Ye, C. S., and Zheng, J. Y.: Long-Term Trends of
855 Anthropogenic SO2, NOx, CO, and NMVOCs Emissions in China, Earth's Future, 6, 1112-1133,
856 10.1029/2018ef000822, 2018.

857 Sutton, M. A., Reis, S., Riddick, S. N., Dragosits, U., Nemitz, E., Theobald, M. R., Tang, Y. S., Braban,
858 C. F., Vieno, M., Dore, A. J., Mitchell, R. F., Wanless, S., Daunt, F., Fowler, D., Blackall, T. D.,
859 Milford, C., Flechard, C. R., Loubet, B., Massad, R., Cellier, P., Personne, E., Coheur, P. F., Clarisse,
860 L., Van Damme, M., Ngadi, Y., Clerbaux, C., Skjoth, C. A., Geels, C., Hertel, O., Wichink Kruit, R. J.,
861 Pinder, R. W., Bash, J. O., Walker, J. T., Simpson, D., Horvath, L., Misselbrook, T. H., Bleeker, A.,
862 Dentener, F., and de Vries, W.: Towards a climate-dependent paradigm of ammonia emission and
863 deposition, Philos Trans R Soc Lond B Biol Sci, 368, 20130166, 10.1098/rstb.2013.0166, 2013.

Van Damme, M., Whitburn, S., Clarisse, L., Clerbaux, C., Hurtmans, D., and Coheur, P.-F.: Version 2 of the IASI NH_3; neural network retrieval algorithm: near-real-time and reanalysed datasets, Atmospheric Measurement Techniques, 10, 4905-4914, 10.5194/amt-10-4905-2017, 2017.

Van Damme, M., Clarisse, L., Whitburn, S., Hadji-Lazaro, J., Hurtmans, D., Clerbaux, C., and Coheur, P. F.: Industrial and agricultural ammonia point sources exposed, Nature, 564, 99-103, 10.1038/s41586-018-0747-1, 2018.

Van Damme, M., Clarisse, L., Heald, C. L., Hurtmans, D., Ngadi, Y., Clerbaux, C., Dolman, A. J., Erisman, J. W., and Coheur, P. F.: Global distributions, time series and error characterization of atmospheric ammonia (NH_3) from IASI satellite observations, Atmospheric Chemistry and Physics, 14, 2905-2922, 10.5194/acp-14-2905-2014, 2014.

Van Damme, M., Clarisse, L., Franco, B., Sutton, M. A., Erisman, J. W., Wichink Kruit, R., van Zanten, M., Whitburn, S., Hadji-Lazaro, J., Hurtmans, D., Clerbaux, C., and Coheur, P.-F.: Global, regional and national trends of atmospheric ammonia derived from a decadal (2008–2018) satellite record, Environmental Research Letters, 16, 10.1088/1748-9326/abd5e0, 2021.

Van Damme, M., Clarisse, L., Dammers, E., Liu, X., Nowak, J. B., Clerbaux, C., Flechard, C. R., Galy-Lacaux, C., Xu, W., Neuman, J. A., Tang, Y. S., Sutton, M. A., Erisman, J. W., and Coheur, P. F.: Towards validation of ammonia (NH_3) measurements from the IASI satellite, Atmospheric Measurement Techniques, 8, 1575-1591, 10.5194/amt-8-1575-2015, 2015.

van der Graaf, S., Dammers, E., Segers, A., Kranenburg, R., Schaap, M., Shephard, M. W., and Erisman, J. W.: Data assimilation of CrIS NH_3; satellite observations for improving spatiotemporal NH_3; distributions in LOTOS-EUROS, Atmospheric Chemistry and Physics, 22, 951-972, 10.5194/acp-22-951-2022, 2022.

van der Werf, G. R., Randerson, J. T., Giglio, L., van Leeuwen, T. T., Chen, Y., Rogers, B. M., Mu, M., van Marle, M. J. E., Morton, D. C., Collatz, G. J., Yokelson, R. J., and Kasibhatla, P. S.: Global fire emissions estimates during 1997–2016, Earth System Science Data, 9, 697-720, 10.5194/essd-9-697-2017, 2017.

Vira, J., Hess, P., Ossohou, M., and Galy-Lacaux, C., 10.5194/acp-2021-538,

Wang, Q., Jacob, D. J., Fisher, J. A., Mao, J., Leibensperger, E. M., Carouge, C. C., Le Sager, P., Kondo, Y., Jimenez, J. L., Cubison, M. J., and Doherty, S. J.: Sources of carbonaceous aerosols and deposited black carbon in the Arctic in winter-spring: implications for radiative forcing, Atmospheric Chemistry and Physics, 11, 12453-12473, 10.5194/acp-11-12453-2011, 2011.

Wang, Y. and Wang, J.: Tropospheric SO2 and NO2 in 2012–2018: Contrasting views of two sensors (OMI and OMPS) from space, Atmospheric Environment, 223, 10.1016/j.atmosenv.2019.117214, 2020.

Warner, J. X., Dickerson, R. R., Wei, Z., Strow, L. L., Wang, Y., and Liang, Q.: Increased atmospheric ammonia over the world's major agricultural areas detected from space, Geophys Res Lett, 44, 2875-2884, 10.1002/2016GL072305, 2017.

Wesely, M.: Parameterization of surface resistances to gaseous dry deposition in regional-scale numerical models☆, Atmospheric Environment, 41, 52-63, 10.1016/j.atmosenv.2007.10.058, 2007.

Whitburn, S., Van Damme, M., Clarisse, L., Bauduin, S., Heald, C. L., Hadji-Lazaro, J., Hurtmans, D., Zondlo, M. A., Clerbaux, C., and Coheur, P. F.: A flexible and robust neural network IASI-NH3retrieval algorithm, Journal of Geophysical Research: Atmospheres, 121, 6581-6599, 10.1002/2016jd024828, 2016.

Xu, W., Zhao, Y., Liu, X., Dore, A. J., Zhang, L., Liu, L., and Cheng, M.: Atmospheric nitrogen deposition in the Yangtze River basin: Spatial pattern and source attribution, Environ Pollut, 232, 546-555, 10.1016/j.envpol.2017.09.086, 2018.

Zhai, S., Jacob, D. J., Wang, X., Liu, Z., Wen, T., Shah, V., Li, K., Moch, J. M., Bates, K. H., Song, S., Shen, L., Zhang, Y., Luo, G., Yu, F., Sun, Y., Wang, L., Qi, M., Tao, J., Gui, K., Xu, H., Zhang, Q., Zhao, T., Wang, Y., Lee, H. C., Choi, H., and Liao, H.: Control of particulate nitrate air pollution in China, Nature Geoscience, 14, 389-395, 10.1038/s41561-021-00726-z, 2021.

Zhang, L., Chen, Y., Zhao, Y., Henze, D. K., Zhu, L., Song, Y., Paulot, F., Liu, X., Pan, Y., Lin, Y., and Huang, B.: Agricultural ammonia emissions in China: reconciling bottom-up and top-down estimates, Atmospheric Chemistry and Physics, 18, 339-355, 10.5194/acp-18-339-2018, 2018.

Zhang, X., Wu, Y., Liu, X., Reis, S., Jin, J., Dragosits, U., Van Damme, M., Clarisse, L., Whitburn, S., Coheur, P. F., and Gu, B.: Ammonia Emissions May Be Substantially Underestimated in China, Environ Sci Technol, 51, 12089-12096, 10.1021/acs.est.7b02171, 2017.

Zhao, Y., Duan, L., Xing, J., Larssen, T., Nielsen, C. P., and Hao, J.: Soil acidification in China: is controlling SO2 emissions enough?, 2009.

Zhao, Y., Zhang, L., Chen, Y., Liu, X., Xu, W., Pan, Y., and Duan, L.: Atmospheric nitrogen deposition to China: A model analysis on nitrogen budget and critical load exceedance, Atmospheric Environment, 153, 32-40, 10.1016/j.atmosenv.2017.01.018, 2017.